AIAA JOURNAL
Vol. 39, No. 6, June 2001

Random Walk Models for Particle Diffusion in Free-Shear Flows

Todd L. Bocksell* and Eric Loth†
University of Illinois at Urbana–Champaign, Urbana, Illinois 61801

The main objectives were to establish and investigate discontinuous and continuous random walk models appropriate for free-shear flows with regard to turbulent particle diffusion. The models were designed to capture the crossing trajectories effect, the continuity effect, and the inertial-limit effect, all for the case of heavy particles whose densities are much greater than that of the surrounding fluid. In addition, both techniques included an isotropic drift velocity to account for inhomogeneous turbulence. The computational efficiency of the continuous random walk models is improved by utilizing local time stepping, which effectively filters out high-frequency velocity fluctuations that do not have a significant influence on particle diffusion. The predictive performances of these two random walk models were examined through comparison with experimental data and idealized test conditions. The results indicate that both models agree well with experimental data for a nearly homogeneous turbulent wake and an inhomogeneous turbulent axisymmetric jet (although the continuous random walk model performs somewhat better for the inhomogeneous flows). It was also found that the proposed drift velocity models are important to ensure continuity when simulating particle diffusion with inhomogeneous turbulence.

Nomenclature

C_c	=	continuity effect coefficient
C_D	=	drag coefficient
C_Λ	=	eddy length scale coefficient
C_μ	=	turbulence length scale coefficient, 0.09
C_τ	=	eddy timescale coefficient
d	=	diameter
Fr	=	eddy Froude number
g	=	gravitational acceleration
h	=	channel width
k	=	turbulent kinetic energy
Re_p	=	particle Reynolds number
St	=	particle Stokes number
t	=	time
$\boldsymbol{u}_i$	=	velocity vector
u'_{fi}	=	discontinuous random walk drift velocity correction
V_{rel}	=	relative velocity of particle to fluid
x_i	=	coordinate/position vector
α_{ij}	=	fluid velocity correlation coefficient
γ	=	drift parameter
Δt	=	time step
δ_{ij}	=	Kronecker delta
$\overline{\delta u'_{fi}}$	=	continuous random walk incremental drift velocity correction
ε	=	turbulent dissipation
Λ_e	=	turbulence integral length scale
ξ	=	random number from triangular probability density function (PDF)
ρ	=	density
σ	=	standard deviation
τ_{int}	=	eddy–particle interaction time
τ_p	=	particle relaxation time
τ_t	=	eddy traversal time
τ_Λ	=	Integral eddy timescale (eddy lifetime)
φ	=	random number from Gaussian PDF

Subscripts

f	=	fluid
i	=	vector
jet	=	jet discharge condition
L	=	Lagrangian
lat	=	lateral
long	=	longitudinal
mE	=	moving Eulerian
p	=	particle
r	=	radial coordinate
z	=	axial coordinate
θ	=	angular coordinate

Superscripts

$\bar{}$	=	Reynolds-averaged component
$'$	=	fluctuating component

Received 27 August 1999; revision received 11 August 2000; accepted for publication 5 January 2001.

*Graduate Research Assistant, Department of Aeronautical and Astronautical Engineering. Student Member AIAA.

†Associate Professor, Department of Aeronautical and Astronautical Engineering. Associate Fellow AIAA.

I. Introduction

A. Particle Diffusion Characteristics

LET us first consider the parameters that control heavy particle diffusion followed by three important features of diffusion phenomena. In general, we assume that the particles are heavy, such that the ratio of particle density to fluid density is large, and are of finite Reynolds number. Therefore, effects of lift, fluid stress, Basset history forces, and Faxen effects are of second-order as compared to drag and gravitational forces.[1] In this case, there are three nondimensional parameters that commonly arise in the analysis of turbulent particle diffusion: the Stokes number St is the ratio of particle relaxation time to eddy integral timescale, the drift parameter γ is the ratio of particle terminal velocity to fluid turbulence intensity, and the eddy Froude number Fr is the ratio of eddy convective forces to gravitational forces on the particle. These three nondimensional parameters can be written as

$$\text{St} = \tau_p/\tau_\Lambda, \qquad \gamma = V_{\text{term}}/u'_{f,\text{rms}}, \qquad Fr = u'^2_{f,\text{rms}}/4g\Lambda_e \tag{1}$$

Two of these three parameters are independent because $\gamma \propto \text{St}/Fr$, and the parameter γ has been shown to be the main parameter controlling long-time particle diffusion in homogeneous, isotropic turbulence.[1–3] In general, particle diffusion becomes equal to that of a passive scalar as γ approaches zero and is substantially reduced as γ becomes large compared to unity.[2,3]

Three important issues associated with turbulent particle diffusion are the crossing-trajectories effect, the continuity effect, and the inertial-limit effect, all of which need to be properly addressed by a computational model to ensure accurate results. Their respective influences are related to the timescale duration of an average eddy interacting with a particle, τ_{int}, which in turn is proportional to mean

diffusion rate for long-time particle diffusion.[1,4,5] Note, for a small tracer particle, this interaction timescale is simply equal to the fluid Lagrangian eddy lifetime $\tau_{\Lambda L}$, because a massless particle follows the Lagrangian fluid path.

The crossing-trajectories effect[1,6–8] refers to the modification of the eddy interaction time that occurs when a particle cuts quickly through an eddy (of length Λ) due to its relative velocity V_{rel} with respect to the fluid. This can result in a net reduction of the interaction time due to the inability of particles to follow the fluid exactly. Therefore, the interaction time is often defined as the minimum of the eddy lifetime and the eddy traversal time as $\tau_{\text{int},i} = \min(\tau_\Lambda, \Lambda/V_{\text{rel}})$ so that the crossing-trajectory effect is more pronounced as particle terminal velocity increases. As the particle–eddy interaction time becomes limited by an eddy traversal time (as opposed to an eddy turnover time), the crossing-trajectories effect yields a reduced overall particle diffusion.

The continuity effect[1–4] refers to the anisotropic nature of the eddy length scale with respect to particle motion, whereby the eddy fluctuations exhibit longer spatial correlations along the particle path as compared to perpendicular to the particle path. Modification of the eddy length scale can subsequently have an effect on the eddy traversal time (discussed earlier), and thus, $\tau_{\text{int},i}$, and the net diffusion can become anisotropic even if the underlying continuous-phase turbulence is isotropic. This effect becomes more important when the relative velocity of the particle is larger than the root mean square of the fluid fluctuation velocities ($\gamma > 1$). In these situations, Taylor's hypothesis is valid, and the Lagrangian correlation is equivalent to the Eulerian spatial correlation moving at the mean fluid velocity. Continuity in terms of the Euler spatial correlation function implies that the lateral correlation functions must have significant negative loops.[9] The resulting anisotropic nature of the correlation functions, thus, leads to the anisotropy in the length scales of the turbulence seen by the particles. For isotropic turbulence, the relationship between the lateral correlation function and the longitudinal correlation function results in[10]

$$\Lambda_{\text{lat}} = \tfrac{1}{2}\Lambda_{\text{long}} \tag{2}$$

The effect of this difference in length scales is that lateral particle diffusion is half of the longitudinal particle diffusion for $\gamma \gg 1$, which is the continuity effect.

The inertial-limit effect[1,4,11–14] refers to the variation in eddy lifetime, which a particle sees along its path, and may be caused by an increase in particle inertia (and, thus, Stokes number). For the case of negligible inertia, the eddy timescale is simply equal to τ_{Λ_L}, but for very high inertia ($\text{St} \gg 1$) and negligible gravity ($\gamma \ll 1$), the eddy timescale approaches the moving Eulerian timescale $\tau_{\Lambda_{mE}}$. (The eddy lifetime along a path that is moving at the mean speed of the fluid.) There is some debate about whether the quantitative values of these two limiting timescales are significantly different. Stock[1] asserts that the ratio of these timescales is ($\tau_{\Lambda_{mE}}/\tau_{\Lambda_L} =$) 2.8. This value is based on the numerical simulation of Wang and Stock[11] using a specific number of Fourier modes to approximate isotropic homogeneous turbulence. However, the fully resolved direct numerical simulation by Elghobashi and Truesdell[14] of the grid-generated turbulence experiment of Snyder and Lumley[15] showed that the timescales for the Lagrangian correlation and the moving Eulerian correlation in zero gravity were nearly identical ($\tau_{\Lambda_{mE}}/\tau_{\Lambda_L} \approx 1$). In addition, Wells and Stock[12] noted experimentally that for zero gravity conditions, increasing the Stokes number only increased diffusion slightly, thus also suggesting the timescale ratio was approximately unity. Finally, an experiment performed by Loth and Stedl[13] measured the Lagrangian and moving Eulerian timescales in a turbulent mixing layer and found that these two scales (when based on the velocity fluctuations) were nearly equal.

Loth and Stedl[13] explained this near equality of timescales in terms of the structural evolution of an eddy. In particular, the transport of a fluid point away from the moving Eulerian path is composed of two motions: an eddy translation and an eddy rotation as shown in Fig. 1. The Lagrangian correlation due to translation alone may be expected to increase the resulting timescale because the eddy is most coherent along its own path as compared to an Eulerian path. However, the effect of the rotational component is that positive velocity fluctuations eventually become negative, resulting in a decorrelation. The two mechanisms have opposite effects and roughly cancel each other out such that the overall correlation of the pure Lagrangian motion is about the same as the moving Eulerian correlation. It is possible that simulation of Wang and Stock,[11] which used a specified number of Fourier modes with random amplitudes and phases and lacks coherent eddy structure, may not include the rotational decorrelation aspect. Based on the preceding discussion, it is reasonable to approximate the two timescales as equal so that the eddy integral timescale will be assumed to be independent of Stokes number. However, further research is needed to clarify this for general turbulent flowfields, especially with respect to inhomogeneous turbulence.

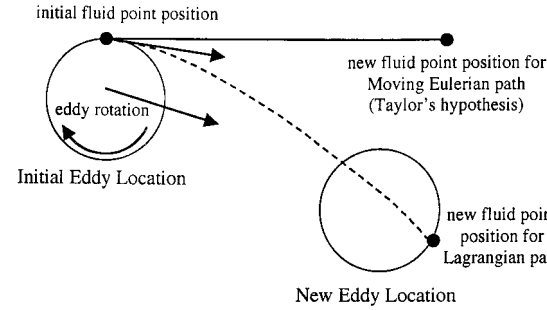

Fig. 1 Movement of a fluid point on an eddy to show the difference between Lagrangian and moving Eulerian correlations.

B. Previous Lagrangian Computational Models

In the event that a resolved-eddy simulation (such as direct numerical simulation or large eddy simulation) is not feasible for the continuous phase, an unresolved-eddy flow simulation, such as a Reynolds-averaged Navier–Stokes (RANS) solution, can be used to obtain results of mean particle diffusion. Whereas the continuous phase is typically described in an Eulerian sense, the particle field can either be treated in an Eulerian or Lagrangian fashion. Lagrangian diffusion models employ the mean flow properties from the RANS solution to compute a large number of particle trajectories and obtain mean diffusion statistics. This methodology can be desirable compared to Eulerian methods because it avoids an empirical particle Schmidt number formulation and can robustly handle particle–wall interaction phenomenon. The Lagrangian stochastic computational models fall into three main categories. These can be arranged from the least computationally intensive to the most computationally intensive as discontinuous random walk (DRW) models, continuous random walk (CRW) models, and stochastic differential equation (SDE) methods. The first two models simulate turbulence by assuming a functional form for the velocity perturbations based on the root-mean-square values of the turbulence. The more complex SDE methods employ a Langevin equation for the instantaneous velocity and require modeling of the triple-velocity moments. In addition, wall interactions cannot be as robustly specified with the SDE methodology. As such this technique is still in the developmental stage and is not yet widely used for most engineering applications.[16]

The DRW model is essentially a zero-dimensional model of the turbulent fluctuations because it approximates the fluctuation as a series of discontinuous velocity perturbations that are held constant during a time interval, as shown in Fig. 2. The CRW model improves the representation of the turbulent fluctuation velocities so that the velocity fluctuations are continuous in time, thus yielding a one-dimensional model (Fig. 2). In both cases, random number generators simulate the chaotic effect that the fluctuating velocities have on particles. For the DRW models these are essentially step changes, whereas the CRW models continuously correlate the turbulent fluid velocity fluctuations in time. Whereas most CRW models employ a Markov chain based on the previous time realization to update after a small time increment, some CRW models, such as the one by Berlemont et al.,[17] include the velocity fluctuation history from many previous time steps.

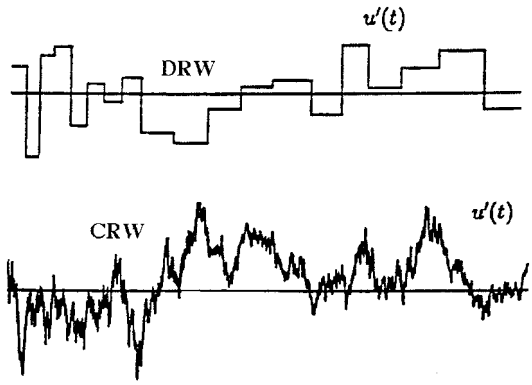

Fig. 2 Comparison of the velocity fluctuation time histories for the DRW and CRW models from MacInnes and Bracco.[6]

For the DRW and CRW approaches with free-shear flows, the k–ε turbulence closure model is typically used for the Eulerian RANS continuous flow solution, from which appropriate length, time, and velocity scales for the continuous flow can be computed based on the turbulent kinetic energy and the dissipation. These turbulence scales are used in conjunction with random number generators to approximate the fluid velocity fluctuations and allow integration of the Lagrangian particle equations of motion. Note that where DRW models typically ignore off-diagonal Reynolds stress terms ($\overline{u'_{f_i} u'_{f_j}}$ for $i \neq j$) in creating the random velocity field that the particle sees, CRW models can include such terms if available from the continuous flow solution.

Recently, MacInnes and Bracco,[6] Crowe et al.,[18] and Legg and Raupach[19] have pointed out serious deficiencies of conventional DRW and CRW models in that they may generate a spurious mean particle drift for inhomogeneous turbulence. This nonphysical drift arises from an inconsistent transformation of Eulerian turbulent statistics into a Lagrangian random walk model that can occur due to gradients along the particle path. For the DRW model, MacInnes and Bracco[6] considered two massless particles approaching each other, but originating from regions of differing turbulence intensities, and their analysis showed that the particles originating from regions of higher turbulence intensity would, on average, diffuse farther than particles originating from regions of lower turbulent intensity. This was numerically demonstrated by releasing a uniform concentration of massless particles (fluid tracers) in an axisymmetric turbulent jet using the DRW, CRW, and SDE methods. The particle concentration distribution was then measured downstream, and instead of a uniform distribution, the random walk models were found to yield nonphysical spatial variations (Fig. 3). This is a result of the spurious mean diffusion of particles from regions of high-turbulence intensity into regions of lower turbulence intensity, which is at the jet edge ($y/x \approx 0.2$–0.3).

To correct this problem, tests were conducted with the addition of a mean drift velocity for a mixing layer and an axisymmetric jet. Results for the latter are shown in Fig. 4 for various DRW and CRW corrections. Based on such results, the transverse mean drift velocity suggested by MacInnes and Bracco[6] for the DRW model for massless particles and isotropic turbulence was

$$\overline{v'_f} = \frac{1}{3}\tau_\Lambda \frac{\partial k}{\partial y} \tag{3}$$

where the $\frac{1}{3}$ factor was based on empirical tests and k is the turbulent kinetic energy. For the CRW model, the suggested drift correction velocity was

$$\overline{\delta u'_{f_i}} = \delta t \frac{\partial \overline{u'_{f_i} u'_{f_j}}}{\partial x_j} \tag{4}$$

which is shown in Fig. 4 to give a reasonably uniform concentration profile for massless particles.

Consequently, the goals of this paper are to establish and evaluate DRW and CRW models for heavy particles in homogeneous and inhomogeneous turbulence through comparison to detailed experimental data and a numerical test flow. The objective is to determine the accuracy and efficiency of these stochastic Lagrangian particle methodologies for simulating turbulent particle diffusion.

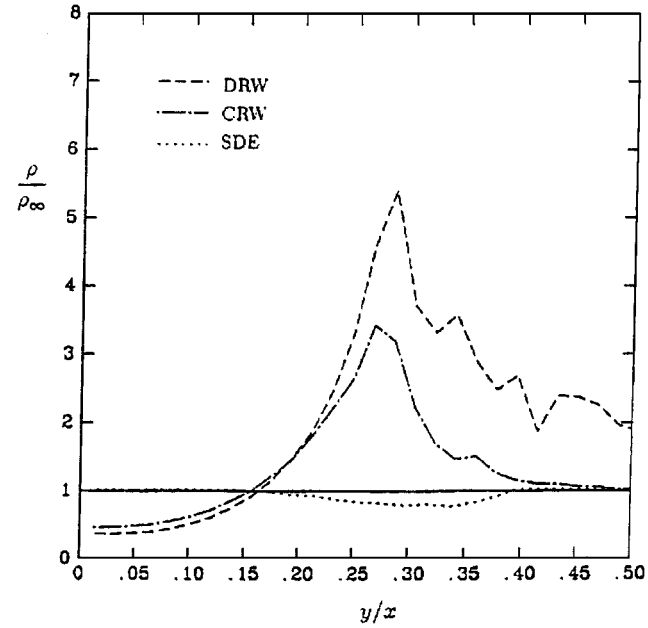

Fig. 3 Radial density profile of an axisymmetric jet showing the effect of neglecting particle drift in the DRW and CRW models (from MacInnes and Bracco[6]).

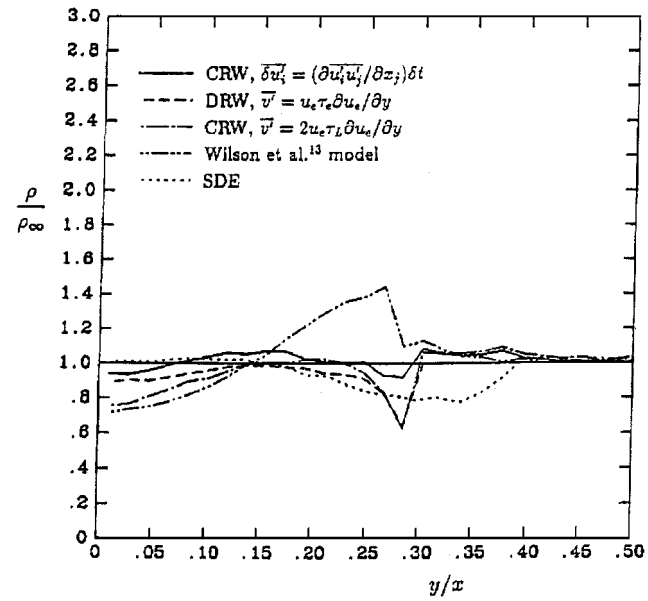

Fig. 4 Radial density profiles in an axisymmetric jet showing the effect of including the particle drift velocity in the DRW and CRW models (from MacInnes and Bracco[6]).

II. Numerical Methodology

A. Continuous-Phase Methodology

In all of the particle simulations to be conducted herein, a description of the continuous-phase flow is first needed. Three turbulent test flows (of increasing complexity) will be considered for evaluation of particle dispersion: 1) a one-dimensional grid-generated decaying wake that is approximately homogeneous and isotropic in the two lateral directions, 2) a numerical test flow with only a transverse variation in the turbulent kinetic energy and is otherwise homogenous, and 3) an inhomogeneous jet flow that encompasses variations in the mean velocity and turbulent variables in both axial and radial directions. These flowfield descriptions are consistent with that

obtained by a conventional isotropic k–ε simulation because this is the most popular RANS flow technique for modeling free-shear flows at high Reynolds numbers. However, the methodology can be extended if anisotropic turbulence characteristics are given. For the isotropic case, the following continuous-fluid variables are required as a function of space (the flow in all cases is assumed to be steady in the mean): mean density ρ_f, viscosity μ, mean Eulerian velocity $\overline{u_{f_i}}$, turbulent kinetic energy k, and dissipation of turbulence ε.

For the three test-case simulations, these Eulerian variables will be obtained as follows: 1) an empirical fit of the experimental data for the grid-generated turbulence, 2) an analytic description for the numerical test flow, and 3) an empirical fit of the experimental data for the jet flow case. Note that empirical fits for cases 1 and 3 were employed instead of RANS simulations because high-quality measurements were available and because this avoided any predictive limitations of the k–ε technique for these flows. This also ensures that differences noted between the numerical and experimental mean particle diffusion results can be attributed solely to the effectiveness of the random walk techniques as opposed to additional limitations of the k–ε model to reproduce correctly the mean and turbulent flow-field distributions. The description of the continuous flow variables for the three test cases is given in the following.

For the first test flow, we utilized the Snyder and Lumley[15] turbulent, grid-generated wake experiment, where the mean flow velocities (meter per second) were experimentally determined to be

$$\bar{w}_f = 6.5, \qquad \bar{u}_f = \bar{v}_f = 0 \tag{5}$$

The measurements also determined that the turbulent kinetic energy and dissipation were nearly one dimensional and well described by the following:

$$k = \tfrac{1}{2}\bar{w}_f^2[1/42.4(z/M - 16) + 2/39.4(z/M - 12)]$$

$$\varepsilon = \tfrac{1}{2}\bar{w}_f^3[1/42.4(z/M - 16)^2 + 2/39.4(z/M - 12)^2]\big/M \tag{6}$$

where z is the distance measured from the grid and M is the grid spacing (2.54 cm). This grid-generated flow was nearly homogeneous in the two directions perpendicular to the flow direction and was nearly isotropic for the domain studied ($68 < z/M < 168$).

For the second test flow, a simple one-dimensional numerical test flow with isotropic inhomogeneous turbulence was designed such that

$$\overline{u_f} = 1, \qquad \overline{v_f} = 0, \qquad k = 0.3\exp[-115(h/2 - y)^2] \tag{7}$$

The domain is defined as $0 \le y/h \le 1$ and periodic in y, and $0 \le x/h \le 15$. This represents a Gaussian distribution of the turbulent kinetic energy in the lateral direction with the peak in the center of the domain as shown in Fig. 5. Dissipation ε was set so that the integral eddy length scale was kept constant throughout the domain at $\Lambda/h = 0.05$.

For the third test flow, the continuous flow solution of an axisymmetric jet was constructed by empirical fit of velocity measurements. The flow in a turbulent axisymmetric jet has three distinct regions consisting of a potential core, a mixing region, and a main region, as shown in Fig. 6. The resulting mean axial and radial fluid velocities for the potential core region of the jet (no turbulence) are

$$\bar{u}_{f_z} = U_{\text{jet}}, \qquad \bar{u}_{f_r} = 0 \tag{8}$$

where U_{jet} is the jet discharge velocity and r and z are the radial and axial jet coordinates. The mean fluid velocity equations for the main region of the jet are

$$U_{\text{centerline}} = \frac{6.8 d_{\text{jet}} U_{\text{jet}}}{z}, \qquad \bar{u}_{f_z} = U_{\text{centerline}}\,\text{sech}^2(a\eta)$$

$$\bar{u}_{f_r} = U_{\text{centerline}}\left\{\eta\,\text{sech}^2(a\eta) + \frac{\ln[\cosh(a\eta)]}{a^2\eta} - \frac{\tanh(a\eta)}{a}\right\} \tag{9}$$

where d_{jet} is the jet nozzle diameter (8 mm), η is the similarity variable r/z, and a is an empirical constant of 10.4 from White.[20] The form for the axial jet velocity in Eq. (9) is recommended by White[20] for a round turbulent jet, and the constant a was obtained by comparison to the data of Wygnanski and Fiedler.[21] The form for the radial jet velocity in Eq. (9) was derived from the axial jet velocity and the continuity equation. Figure 7 shows a comparison

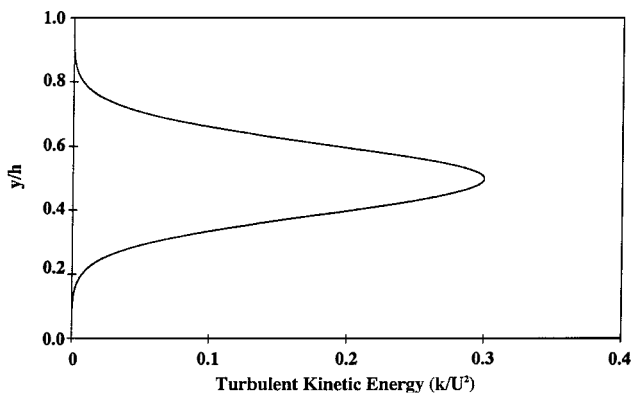

Fig. 5 Distribution of turbulent kinetic energy used in the numerical test flow to evaluate the correction velocities.

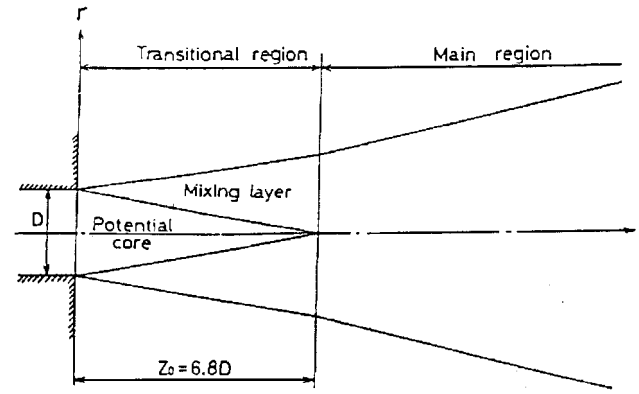

Fig. 6 Three regions of a turbulent axisymmetric jet (from Yuu et al.[22]).

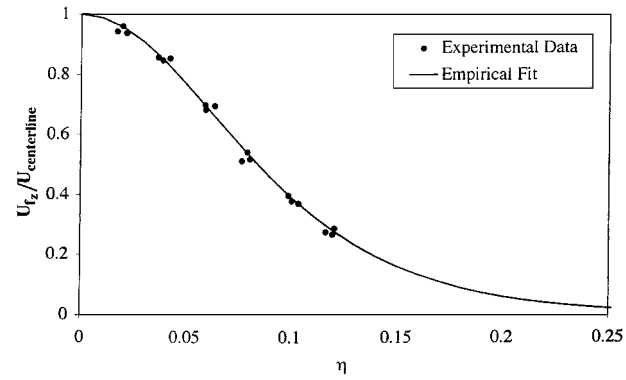

Axial velocity

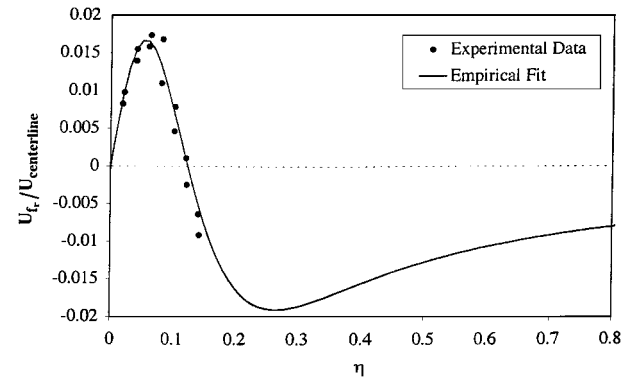

Radial velocity

Fig. 7 Comparison of experimental data for an axisymmetric jet and corresponding empirical equations (9).

between the empirical equations for the axial and radial velocities in an axisymmetric jet to the experimental data presented by Yuu et al.[22] The equations for the mean velocities in the mixing layer were similar except that the maximum velocity is no longer located exactly at $r=0$, but extends to the edge of the potential core as described by Bocksell.[23] The time spent in the potential core and mixing regions of the jet was small compared to the time spent in the main region, and so it is not imperative to model these regions exactly; this approach is thus deemed reasonable.

The turbulent kinetic energy is obtained from the empirical equations given by Yuu et al.[22] for the mean-square velocity fluctuations in each coordinate direction for the mixing region and jet region. After computing the turbulent kinetic energy from these autocorrelations, the isotropic dissipation is computed from k, using

$$\varepsilon = C_\mu k^2 \big/ \nu_t \tag{10}$$

where ν_t is an eddy viscosity model for a turbulent axisymmetric jet based on that of Anderson et al.[24] as described by Bocksell.[23]

B. Particle Equations of Motion

The equations of motion governing a particle in a turbulent flow can be written in each Cartesian coordinate $\hat{i}$ as

$$\frac{\mathrm{d}x_{p_i}}{\mathrm{d}t} = u_{p_i} \tag{11}$$

where x_{p_i} is the particle position and u_{p_i} is the particle velocity. The equation for the particle velocity is given by Maxey and Riley[25] as

$$\mathrm{Vol}_p \rho_p \frac{\mathrm{d}u_{p_i}}{\mathrm{d}t} = F_{D_i} + F_{BG_i} + F_{VM_i} + F_{BH_i} + F_{SG_i} \tag{12}$$

where Vol_p is the particle volume and ρ_p is the particle density. The forces on the right-hand side of Eq. (12) are the drag force F_{D_i}, the buoyancy-gravitational force F_{BG_i}, the virtual mass force F_{VM_i}, the Basset history force F_{BH_i}, and the force due to stress gradients in the fluid F_{SG_i}. The stress gradient force is due to a combination of the fluid shear stress gradient and the fluid pressure gradient. In the limit of a heavy particle ($\rho_p \gg \rho_f$), forces associated with virtual mass, Basset history, and stress gradients (including shear stress and pressure) are typically negligible,[2,7] and Eq. (12) simplifies to

$$\frac{\mathrm{d}u_{p_i}}{\mathrm{d}t} = \frac{3}{4d_p}\frac{\rho_f}{\rho_p}\left|u_{f_i} - u_{p_i}\right|\left(u_{f_i} - u_{p_i}\right)C_D + \boldsymbol{g}_i \tag{13}$$

where d_p is the particle diameter, $\boldsymbol{g}_i$ is the gravitational acceleration vector, and u_{f_i} is the instantaneous fluid velocity. The same nonlinear C_D used by DeAngelis et al.[26] is utilized here and has the form

$$C_D = \begin{cases} (24/Re_p)\left(1 + \frac{1}{6}Re_p^{\frac{2}{3}}\right) & Re_p \le 1000 \\ 0.424 & Re_p > 1000 \end{cases} \tag{14}$$

The particle trajectory is then obtained by integrating Eqs. (11) and (13). However, the instantaneous fluid velocity in Eq. (13) includes both a mean and fluctuating component of velocity, $u_{f_i} = \overline{u_{f_i}} + u'_{f_i}$. A RANS-type flow provides the mean fluid velocity $\overline{u_{f_i}}$, thus requiring separate modeling of the fluid fluctuation velocity u'_{f_i} at the Lagrangian particle location. The two techniques to obtain the fluctuation fluid velocity are the DRW and CRW models (described in the following sections) and are based on the Eulerian continuous-fluid distribution. In both techniques, the mean velocity of the fluid is obtained by simply sampling $\overline{u_{f_i}}$ at the particle location.

C. DRW Methodology

There have been several studies employing DRW models since the earliest models proposed by Gosman and Ioannides[8] and Yuu et al.[22] Further refinement and sophistication by Schuen et al.[7] and DeAngelis et al.[26] improved the overall performance, but the robustness was still a concern. Herein, the best features of these previous models along with some new ideas have been combined to design a DRW model that is intended to be capable of simulating particle diffusion for a wider variety of engineering flows.

The basic principle of a DRW model is that a particle interacts with a series of eddies representing the fluctuating component of the fluid velocity. For this DRW model, the fluid velocity fluctuations can be computed by stochastically sampling an anisotropic Gaussian distribution along the particle path as

$$u'_{f_i}(t) = \sigma_{u_i}\varphi_i + \overline{u'_{f_i}}, \qquad \text{with} \qquad \sigma_{u_i} = \left(\overline{u'^2_{f_i}}\right)^{\frac{1}{2}} \tag{15}$$

where φ_i is a Gaussian random number and $\overline{u'_{f_i}}$ is a mean drift velocity required to obtain proper transformation from Eulerian statistics to the Lagrangian path for inhomogeneous turbulence (which will be discussed in Sec. II.E).

At the onset of a new eddy, φ_i is sampled for each particle, and Eq. (15) is computed at every time step by holding φ_i constant but updating σ_{u_i} to correspond with the flow conditions at the current particle location, which can be important for an inhomogeneous flow. This procedure allows $u'_{f_i}(t)$ to vary throughout the eddy–particle interaction time interval. From this, the particle equations of motion are integrated in time until the particle will no longer interact with each particular zero-dimensional eddy that occurs when $t > \tau_{\mathrm{int}}$. Defining the eddy–particle interaction time as a function of the eddy lifetime and the eddy traversal time captures the crossing-trajectories effect; therefore,

$$\tau_{\mathrm{int},i} = \min(\tau_\Lambda, \tau_{t,i}) \tag{16}$$

where $\tau_{t,i}$ is the eddy traversal time. We have found that the empirical expression for $\tau_{\mathrm{int},i}$ used in Eq. (16) provides a somewhat better prediction with experiment than the more smoothly varying expression, $\tau_{\mathrm{int}}^{-2} = \tau_\Lambda^{-2} + \tau_{t,i}^{-2}$ suggested by Csanady.[4]

In Eq. (16), τ_Λ and $\tau_{t,i}$ are computed from the RANS gas-phase solution as

$$\tau_\Lambda = C_\tau \xi (k/\varepsilon), \qquad \tau_{t,i} = \Lambda_i / V_{\mathrm{rel}}$$

with

$$\Lambda_i = C_{c,i} C_\Lambda C_\mu^{\frac{3}{4}} \left(k^{\frac{3}{2}} \big/ \varepsilon\right), \qquad C_{c,i} = 1 + V_{\mathrm{rel},i}/|V_{\mathrm{rel},i}| \tag{17}$$

where ξ is a random number. The inclusion of randomness in the calculation of the eddy lifetime is necessary for particles that have an eddy interaction time exclusively governed by the eddy lifetime. Without this randomness, particles governed by the eddy lifetime may tend to enter and exit eddies synchronously in time, leading to particle diffusion results that are not physically realizable. The value for ξ is obtained by sampling from a triangular probability density function (PDF) ranging from $0.1\tau_\Lambda$ to $1.9\tau_\Lambda$ with a mean value of τ_Λ. However, results by Bocksell[23] showed that the size and shape of the PDF were not critical, as long as some randomness is introduced. Also present in Eq. (17) are four coefficients: C_μ is the standard coefficient of the k–ε model (0.09), C_τ and C_Λ are empirical coefficients of the DRW model and will be described later, and $C_{c,i}$ is the continuity effect coefficient. Schuen et al.[7] notes that due to the arbitrary definitions for eddy length and timescales, C_τ and C_Λ require calibration for accurate results.

Contrary to a model proposed by Stock,[1] the eddy lifetime is herein independent of St because we have assumed that $\tau_{\Lambda L} \approx \tau_{\Lambda mE}$, in describing the inertial-limit effect (see Sec. I.A). The implementation of the continuity effect through $C_{c,i}$ is similar to the model of Graham[27] except that the present model is not limited to particles moving at a nearly terminal velocity. This difference can be important when an initial velocity is given to a particle such that gravitational forces do not primarily govern V_{rel}.

D. CRW Methodology

The CRW model is a more qualitatively realistic representation of turbulence than the DRW model. In the CRW model, the fluid velocity fluctuations along a particle path are approximated with a random walk model that is continuous in time by utilizing a Markov chain between two time steps as

$$u'_{f_i}(t + \Delta t) = \alpha_{ij} u'_{f_j}(t) + \left\{\left(\delta_{ij} - \alpha_{ij}^2\right)\sigma_{u_j}^2\right\}^{\frac{1}{2}}\varphi_i + \delta\overline{u'_{f_i}} \tag{18}$$

where φ_i is a Gaussian random number sampled at each time step (as compared to the DRW model where it is sampled every $\tau_{\text{int},i}$). Again, $\delta u'_{f_i}$ is a mean drift velocity along the particle arising for inhomogeneous turbulence (which will be discussed in Sec. II.E).

In the general case of inhomogeneous, anisotropic turbulence with a RANS flow solution that solves for the complete Reynolds-stress tensor statistics,

$$\alpha_{ij} = \frac{\overline{u'_{f_i} u'_{f_j}}}{\left\{\left(\overline{u'^2_{f_i}}\right)\left(\overline{u'^2_{f_j}}\right)\right\}^{\frac{1}{2}}} \exp\frac{-\Delta t}{\tau_{\text{int},i}}, \qquad \sigma_{u_j} = \left(\overline{u'^2_j}\right)^{\frac{1}{2}} \tag{19}$$

Note the timescale used is the particle–eddy interaction time because this governs the fluctuation decorrelation along the particle path. The omission of the off-diagonal stress terms ($\overline{u'_{f_i} u'_{f_j}} = 0$ for $i \neq j$) is appropriate for homogeneous, isotropic turbulent flows and is typically a second-order effect for thin shear layer flows. Neglecting the off-diagonal stress terms also allows direct comparison with the DRW model (where they are typically not included).

Therefore, the present CRW correlation employed herein is simply given as

$$\alpha_{ij} = \delta_{ij} \exp(-\Delta t/\tau_{\text{int},i}), \qquad \sigma_{u_j} = \left(\tfrac{2}{3}k\right)^{\frac{1}{2}} \tag{20}$$

where we have assumed isotropic turbulence intensities. In Eqs. (19) and (20), $\tau_{\text{int},i}$ is computed similarly to the DRW model by utilizing Eqs. (16) and (17). One difference is, in computing the eddy lifetime, the CRW model uses $\tau_\Lambda = C_\tau k/\varepsilon$, and the random variable ξ of the DRW model is no longer included, nor is it necessary. Also for the CRW model, $\tau_{\text{int},i}$ is computed at every time step rather than at the onset of each new eddy for the DRW model. Note that the CRW model of Legg and Raupach,[19] which is discussed by Chen and Pereira,[28] decreases σ_{u_j} with increasing particle Stokes number. Herein, σ_{u_j} is independent of particle Stokes number and is typical for most CRW models.[2] This is because particles in homogeneous turbulence experience similar fluid fluctuation velocity magnitudes regardless of the speed of the particle through the fluid.

To improve the efficiency of the present CRW model, the high-frequency fluctuations that do not significantly contribute to particle diffusion can be filtered out. This filtering can significantly reduce CPU and is accomplished by defining a local time step to be a function of the eddy interaction timescale as

$$\Delta t = |\tau_{\text{int},i}|/N_{\text{cutoff}} \tag{21}$$

The minimum acceptable value of N_{cutoff} was determined with several simulations by matching the lateral diffusion to within 1% of that found using the statistically converged global time step for particles in homogeneous isotropic turbulence.[23] The results shown in Fig. 8a exhibited rapid convergence to the global time-stepping diffusion curve when N_{cutoff} is eight or greater. This is less than the N_{cutoff} required for the DRW model of Bocksell.[23] This may be because the CRW model introduces velocity randomness at every time step compared to every $\tau_{\text{int},i}$ for the DRW model.

An interesting feature of the acceleration scheme for the CRW model is the resulting spectra of the turbulence seen by the particles. Figure 8b shows a comparison of the spectra of the fluctuation seen by particles for two disparate values of N_{cutoff}, 8 and 2048. The decay of velocity fluctuations with respect to frequency for this Markov model is approximately linear up to the low-pass frequency. In addition, $N_{\text{cutoff}} = 8$ has only captured the fluctuations associated with the largest wavelengths; however the resulting mean-square diffusion curves for these two spectra are nearly identical.

E. Inhomogeneous Drift Velocity

MacInnes and Bracco,[6] Legg and Raupach,[19] and Iliopoulos and Hanratty[29] all have shown that a drift velocity arises for inhomogeneous turbulence. MacInnes and Bracco[6] studied massless particles (fluid elements) in a jet and a shear layer and noted that neglecting the mean drift velocity in Eqs. (15) and (18) can lead to significant errors.

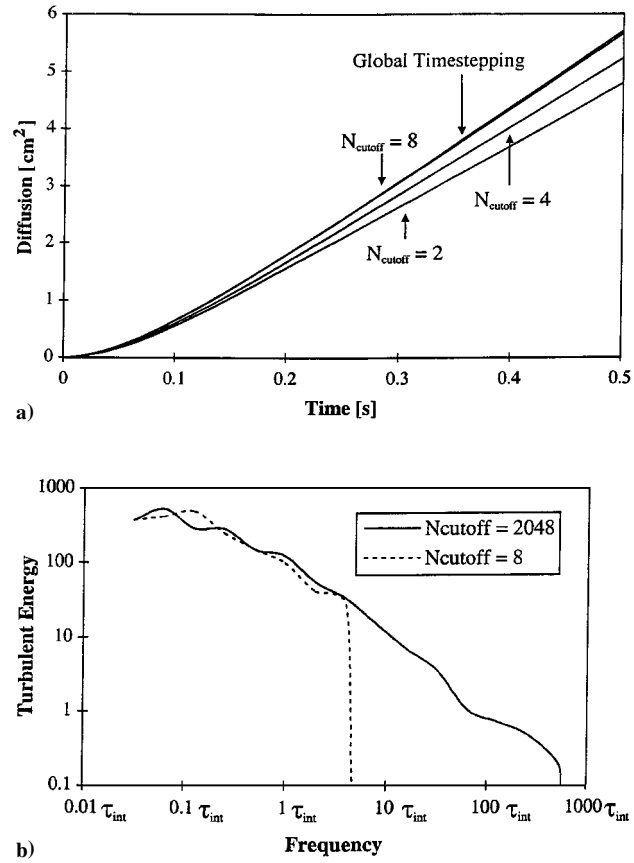

Fig. 8 CRW simulations of a) mean-square diffusion for various values of N_{cutoff} and b) comparison of the spectra of the velocity fluctuations for the CRW model for two disparate values of N_{cutoff}.

The isotropic drift velocity corrections employed herein are derived to show their genesis. The definition of the Lagrangian derivative of the fluid velocity along the fluid path is given by

$$\frac{\mathrm{D}u_{f_i}}{\mathrm{D}t} = \frac{\partial u_{f_i}}{\partial t} + u_{f_j}\frac{\partial u_{f_i}}{\partial x_j} \tag{22}$$

and taking the time average for stationary flow yields

$$\frac{\overline{\mathrm{D}u_{f_i}}}{\mathrm{D}t} = \overline{u}_{f_j}\frac{\partial \overline{u}_{f_i}}{\partial x_j} + \overline{u'_{f_j}\frac{\partial u'_{f_i}}{\partial x_j}} \tag{23}$$

or, equivalently,

$$\frac{\overline{\mathrm{D}u_{f_i}}}{\mathrm{D}t} = \frac{\mathrm{D}\overline{u}_{f_i}}{\mathrm{D}t} + \frac{\overline{\mathrm{D}u'_{f_i}}}{\mathrm{D}t}$$

where

$$\frac{\overline{\mathrm{D}\overline{u}_{f_i}}}{\mathrm{D}t} = \overline{u}_{f_j}\frac{\partial \overline{u}_{f_i}}{\partial x_j}, \qquad \frac{\overline{\mathrm{D}u'_{f_i}}}{\mathrm{D}t} = \overline{u'_{f_j}\frac{\partial u'_{f_i}}{\partial x_j}} \tag{24}$$

For the net change in the fluid velocity over a time Δt (fluid acceleration), we note that the first term on the right-hand side of Eq. (23) is taken into account by simply sampling $\overline{u}_{f_i}$ along the fluid path. For example,

$$\frac{\overline{\mathrm{D}\overline{u}_{f_i}}}{\mathrm{D}t} \approx \frac{\overline{u}_{f_i}\left(x_{f_i} + \Delta x_{f_i}, t + \Delta t\right) - \overline{u}_{f_i}\left(x_{f_i}, t\right)}{\Delta t} \tag{25}$$

The second term on the right-hand side of Eq. (23), however, is nonzero if the turbulence is inhomogeneous and must be included to represent properly the fluid acceleration along a fluid path. Note that this term is only nonzero in a Lagrangian reference frame.

The contribution to overall fluid acceleration by the inhomogeneity of the turbulence is accomplished through the addition of a mean drift velocity to the fluctuation component of the fluid velocity in

the DRW and CRW models (15) and (18). For the DRW model, discretization of the third term of Eq. (24) yields the time-evolving equation for the mean drift velocity $\overline{u'_{fi}}$ of fluid elements for inhomogeneous turbulence:

$$\overline{u'_{fi}}(t+\Delta t) = \overline{u'_{fi}}(t) + \Delta t\left(\overline{u'_{fj}\frac{\partial u'_{fi}}{\partial x_j}}\right) \tag{26}$$

For specific flows, the physics may be able to provide insight into which terms in Eq. (26) are important and which can be neglected, thus providing a more convenient form for the drift velocity equation. For thin free-shear flows, such as a jet, the last term on the right-hand side of Eq. (26) will be dominated by $\overline{v'_f \partial v'_f/\partial y}$, and assuming isotropy (typical for DRW models), the transverse drift velocity component for massless particles becomes

$$\overline{v'_f}(t+\Delta t) = \overline{v'_f}(t) + \Delta t\frac{1}{3}\frac{\partial k}{\partial y} \tag{27}$$

The DRW drift velocity of Eq. (27) for a fluid element is similar to the isotropic version of the CRW drift velocity of MacInnes and Bracco[6] but is quite different from their DRW drift velocity in Eq. (3). Note that their DRW model will only predict the same drift as that of Eq. (27) when $\sum \Delta t = \tau_\Lambda$ for a constant gradient flow. As such, the semi-empirical DRW drift velocity of MacInnes and Bracco,[6] given by Eq. (3) is expected to overpredict drift velocity at short times, $t < \tau_\Lambda$, and underpredict drift velocity at long times, $t > \tau_\Lambda$.

Note that the DRW drift corrections of Eqs. (26) and (27) assume that the gradients along a streamline are constant. When this assumption is not reasonable, an additional drift correction term of the form $(\Delta t^2/2)(\mathrm{D}/\mathrm{D}t)(\partial k/\partial x_i)$ may be included. For example, this correction can be important when particles convect from regions of high-turbulence gradients to negligible-turbulence gradients in which case Eqs. (26) and (27) retain a nonzero drift velocity when in fact the drift velocity should decay to zero. Notably, the DRW drift velocity of MacInnes and Bracco[6] [Eq. (3)] retains the correct qualitative decay under these conditions, but is not quantitatively accurate under general conditions (as will be shown in the next section).

For the CRW model, an incremental change ($\delta\overline{u'_{fi}}$) in the velocity fluctuation equation (18) is considered because the velocity fluctuations are continuous in time, unlike the DRW model. This incremental change is derived similarly to Eq. (26) yielding the incremental drift velocity for the CRW model as

$$\delta\overline{u'_{fj}} = \Delta t\left(\overline{u'_{fj}\frac{\partial u'_{fi}}{\partial x_j}}\right) \tag{28}$$

which is equivalent to Eq. (4). For the transverse component of velocity for thin free-shear flows, where one can assume isotropic turbulence Eq. (28) becomes

$$\delta\overline{v'_f} = \Delta t\frac{1}{3}\frac{\partial k}{\partial y} \tag{29}$$

Note that the CRW drift correction of Legg and Raupach[19] is

$$\delta\overline{v'_f} = \tau_\Lambda\left[1-\exp\left(\frac{-\Delta t}{\tau_\Lambda}\right)\right]\frac{\partial}{\partial y}\left(\sigma_v^2\right) \tag{30}$$

and to first order, Eq. (30) is equivalent to Eq. (29) for isotropic turbulence.

Now let us consider the drift velocity for finite mass particles, where the particle Lagrangian path no longer necessarily coincides with the fluid Lagrangian path. In this case, we must consider the derivative of the fluctuating fluid velocity along the particle path

$$\frac{\mathrm{d}u_{fi}}{\mathrm{d}t} = \frac{\partial u_{fi}}{\partial t} + \left(u_{pj}\right)\frac{\partial u_{fi}}{\partial x_j} \tag{31}$$

Taking the time average, we have

$$\overline{\frac{\mathrm{d}u_{fi}}{\mathrm{d}t}} = \overline{u_{pj}}\frac{\partial\overline{u_{fi}}}{\partial x_j} + \overline{u_{pj}\frac{\partial u'_{fi}}{\partial x_j}} \tag{32}$$

or, equivalently,

$$\overline{\frac{\mathrm{d}u_{fi}}{\mathrm{d}t}} = \overline{\frac{\mathrm{d}\overline{u_{fi}}}{\mathrm{d}t}} + \overline{\frac{\mathrm{d}u'_{fi}}{\mathrm{d}t}}$$

$$\text{where}\qquad \overline{\frac{\mathrm{d}\overline{u_{fi}}}{\mathrm{d}t}} = \overline{u_{pj}}\frac{\partial\overline{u_{fi}}}{\partial x_j}, \qquad \overline{\frac{\mathrm{d}u'_{fi}}{\mathrm{d}t}} = \overline{u_{pj}\frac{\partial u'_{fi}}{\partial x_j}} \tag{33}$$

Thus similar to the situation of a fluid element, the net change in the fluid velocity over time along the particle path involves two components. The first term on the right-hand side of Eq. (32) is taken into account by sampling $\overline{u_{fi}}$ along the particle path. For example,

$$\overline{\frac{\mathrm{d}\overline{u_{fi}}}{\mathrm{d}t}} \approx \frac{\overline{u_{fi}}\left(x_{p_i}+\Delta x_{p_i}, t+\Delta t\right) - \overline{u_{fi}}\left(x_{p_i}, t\right)}{\Delta t} \tag{34}$$

The second term on the right-hand side of Eq. (32) is again nonzero for inhomogeneous turbulence and should be included in the DRW and CRW models of the fluctuation fluid velocities provided along the particle path. One may relate this correction to that for a fluid tracer by using the isotropic correlation of Tu and Fletcher[30] modified to include the crossing-trajectories effect, noted in Eq. (19), whereby

$$\overline{u'_{pi}u'_{fi}} = \overline{u'_{fi}u'_{fi}}\exp(-B_k\gamma) \tag{35}$$

where B_k (=0.09) was determined from experimental data of Tu and Fletcher.[30] From this, we note that, for $\gamma \ll 1$ (which is true for the conditions employed herein), one may reasonably employ the drift correction for a massless particle.

In summary, three drift corrections are investigated herein for isotropic turbulence in thin free-shear layer flows with particles of low γ: the DRW drift of MacInnes and Bracco[6] in Eq. (3), the analytically based DRW drift correction of Eq. (27), and the analytically based CRW drift correction of Eq. (29).

III. Test Flow Results

Validation of the models in the heavy particle limit ($\rho_p \gg \rho_f$) was performed using two basic free-shear turbulent flows (a nearly homogeneous wake and an inhomogeneous axisymmetric jet) for which detailed heavy particle experimental data are available. In addition, the drift correction terms of Eqs. (27) and (29) were validated through simulations of tracer particles in an idealized one-dimensional inhomogeneous channel flow and an empirical two-dimensional inhomogeneous jet flow. The number of particles used in each simulation was varied over a significant range to ensure statistical convergence. The time steps were also kept uniform for the CRW simulations and were sufficiently small to provide accurate temporal resolution.

For the first test flow, we utilized the Snyder and Lumley[15] grid-generated wake experiment where the mean-square diffusion of four types of particles (see Table 1) was measured. The particle diffusion (based on the root mean square of the transverse particle locations) was measured over the range $z/M = 68.4$–168 in both the experiments and the present simulations. This grid-generated flow is nearly homogeneous, thus allowing the drift correction terms to be neglected. The coefficients for the eddy timescale and length scale,

Table 1 Characteristics of the four particle types used in the Snyder and Lumley[15] grid-generated turbulence experiment

Particle type	Particle radius, μm	Particle density, kg/m^3	Initial τ_p, s	Terminal velocity, m/s
Hollow glass	23.25	260	0.00174	0.0167
Corn pollen	43.5	1000	0.0223	0.198
Solid glass	43.5	2500	0.0557	0.442
Copper	23.25	8900	0.0594	0.483

Table 2 Calibrated coefficients for the DRW and CRW models

Coefficient	DRW	CRW
C_τ	0.21	0.27
C_Λ	1.8	1.6

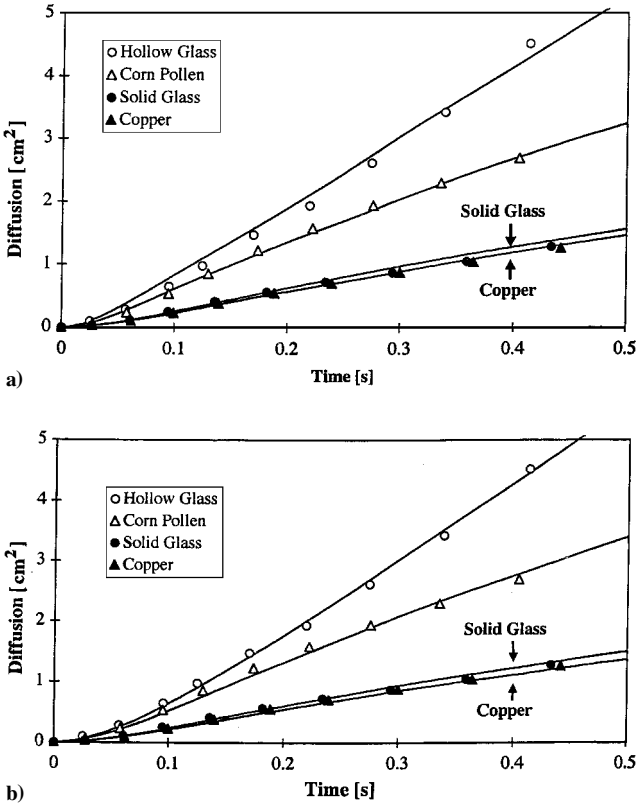

Fig. 9 Comparison of numerical results of diffusion in grid-generated turbulence to the experiment of Snyder and Lumley[15] for a) DRW and b) CRW simulations.

appearing in the CRW model as C_τ and C_Λ, were calibrated to agree with the particle diffusion results. The resulting values for the DRW and CRW models are presented in Table 2. Figure 9 shows the comparison of the DRW and CRW simulations, respectively, of particle diffusion to the data of Snyder and Lumley.[15] The agreement for both models is quite good for short-time and long-time diffusion indicating that both models include the basic features to simulate homogeneous turbulent particle diffusion (although the CRW results are slightly better).

For the second test flow, the importance of the spurious drift correction terms for massless particles was investigated with a simple one-dimensional flow with isotropic inhomogeneous turbulence as specified in Eq. (7). Because the mean flow is divergence free, a uniform initial distribution of tracer particles in the transverse direction at $x/h = 0$ should remain uniform in concentration while convecting downstream.[6] To test this, particles of negligible radius were injected uniformly at the inlet ($x/h = 0$) and the resulting density profiles were computed at various planes downstream. It was determined that 50,000 particles were sufficient for the numerical test flow study.

Figure 10a shows the normalized density profiles at x/h locations of 1, 5, 10, and 15 for the DRW model with no drift correction velocity included. There is a dramatic accumulation of particles at the edges of the domain corresponding to locations in the flow where the turbulent kinetic energy is minimum, and this accumulation worsens as x/h increases. Figure 10b shows a similar trend, although not as exaggerated, for the CRW model without a drift correction. These results are qualitatively similar to those found by MacInnes and Bracco[6] for the axisymmetric jet (Fig. 4). Figure 11 shows the result of including the drift correction velocities. The

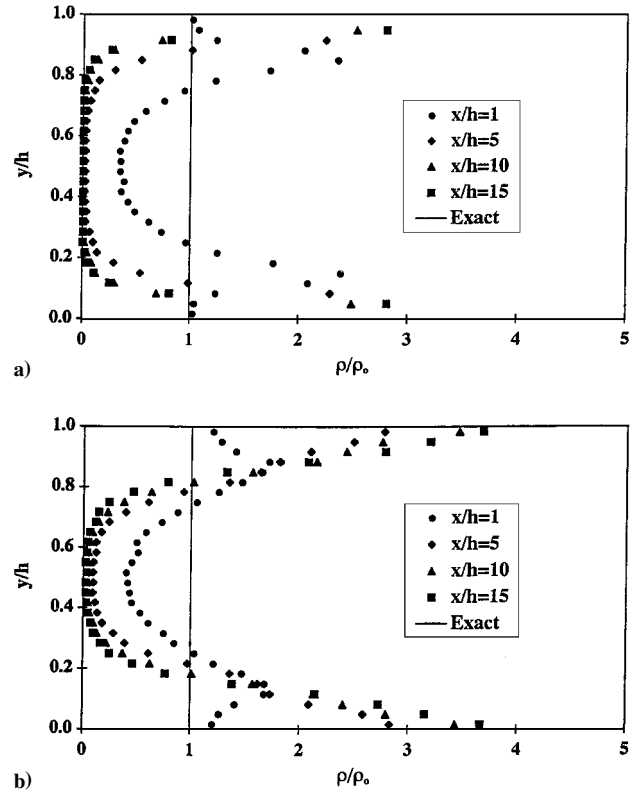

Fig. 10 Tracer particle concentration profiles of the numeric test flow at four downstream locations without drift correction velocities for a) DRW and b) CRW model.

DRW results using the semi-empirical drift correction of MacInnes and Bracco are shown in Fig. 11a and the proposed drift velocity of Eq. (27) are shown Fig. 11b. The drift velocity of MacInnes and Bracco clearly worsened downstream (where $t > \tau_\Lambda$). This is consistent with the expected underprediction of drift velocity for this model as described in Sec. II.E. In contrast, the scalar concentration across the channel for the proposed DRW drift velocity of Eq. (27) remains nearly uniform downstream. Figure 11c shows the normalized density profiles for CRW model including the drift velocity increment of Eq. (29). The resulting density profiles remain nearly uniform at all downstream locations and are generally better than that for the DRW model proposed herein for this type of flow.

For the third test flow, the drift correction terms are evaluated in a two-dimensional inhomogeneous turbulent jet flow with tracer particles. The tracer particles are injected uniformly with respect to fluid volume flux at a location in the main region of the jet ($z/d_{\text{jet}} = 10$). The motion of the tracer particles is computed, and density profiles are obtained at five planes ($z/d_{\text{jet}} = 10$, 15, 20, 25, and 30). Similarly to the earlier channel flow, the mean flow is divergence free and a uniform initial distribution of tracer particles will remain uniform. It was determined that 200,000 particles were sufficient for these simulations.

Figure 12a shows the normalized density profiles in the jet at the five z/d_{jet} locations for the DRW model without the drift velocity. There is an accumulation of particles at the outer edge of the jet (low-turbulence intensity) and a depletion of particles from the center of the jet (high-turbulence intensity) similar to the results from the channel flow. The same trend appears for the CRW model without the drift velocity and is shown in Fig. 12b. Figure 13a shows the normalized density profiles for the DRW model with the drift velocity of MacInnes and Bracco,[6] where it is evident that continuity is not satisfied. Figure 13b shows the normalized density profiles for the CRW model with the proposed drift velocity of Eq. (29), where the density profiles remain nearly uniform at all collection planes (close to the exact solution) and are superior to the results of the DRW model with either drift correction. The results for the DRW drift given by Eq. (27) tended to give nonphysical concentration peaks at the center of the jet (not shown). This is due to some

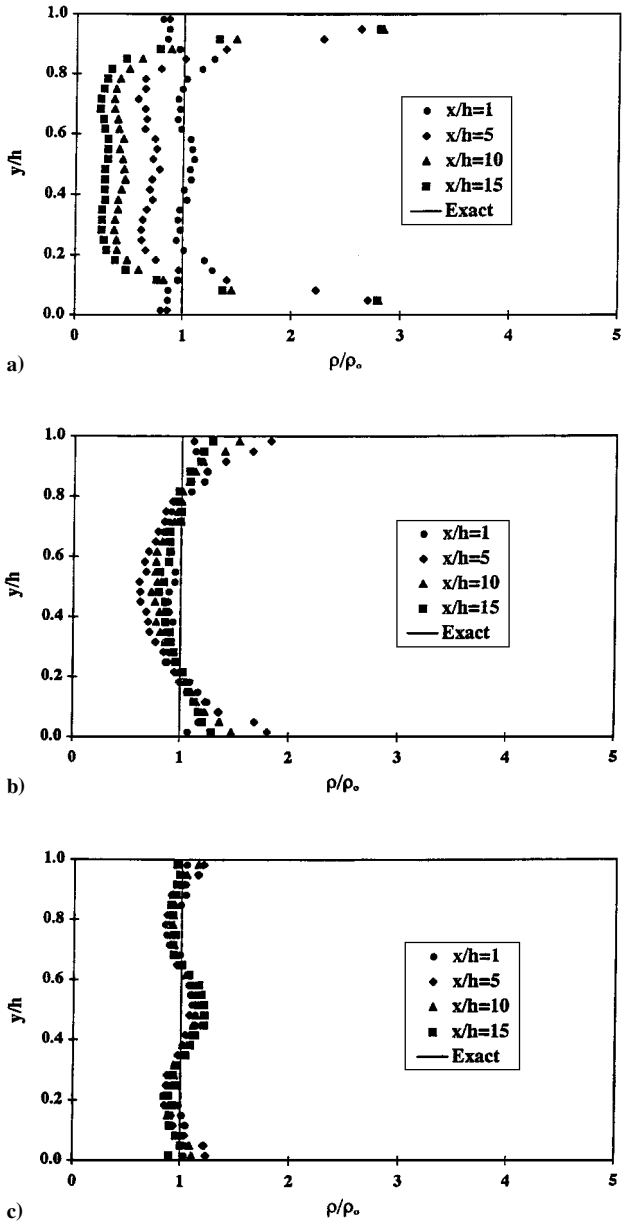

Fig. 11 Tracer particle concentration profiles for the numeric test flow at four downstream locations for a) DRW model with drift velocity proposed by MacInnes and Bracco,[6] b) DRW model with the proposed drift velocity of Eq. (27), and c) CRW model with the proposed drift velocity of Eq. (29).

of the tracer particles convecting from high-turbulence gradients to low-turbulence gradients and artificially retaining a drift velocity, an issue discussed in Sec. II.E.

For the fourth test flow, heavy (nontracer) particle diffusion in an axisymmetric jet was simulated to compare with concentration measurements of Yuu et al.[22] The fluctuation velocities from the DRW and CRW models were sampled from the mean velocity fluctuation intensities in each direction. At least 50,000 particles (in conjunction with 15 collection bins evenly distributed in the radial direction) were used to compute the particle concentration profiles. The particle initial conditions for the axisymmetric jet were computed by Schuen et al.[7] and proved to be slightly different than the jet discharge velocities. Overall, there were two particle sizes used in the Yuu et al.[22] experiment along with three jet discharge velocities to generate three experimental testing conditions (see Table 3). Yuu et al.[22] gives the experimental combination of particle sizes and jet discharge velocities used. For these testing conditions, the tracer drift correction velocities of Eqs. (27) and (29) were utilized for the DRW and CRW models. This is a valid approximation for these nontracer particles, because even for the largest particles simulated in the jet, the average γ along the particle paths was less than 10%,

Table 3 Particle and jet characteristics for the three testing conditions of the Yuu et al.[22] axisymmetric jet experiment

Initial particle Stokes number	Particles radius, μm	Particle density, kg/m^3	Jet velocity, m/s	Particle velocity, m/s
3.4	7.5	2000	20	14
15	10	2000	50	30
30	10	2000	100	54

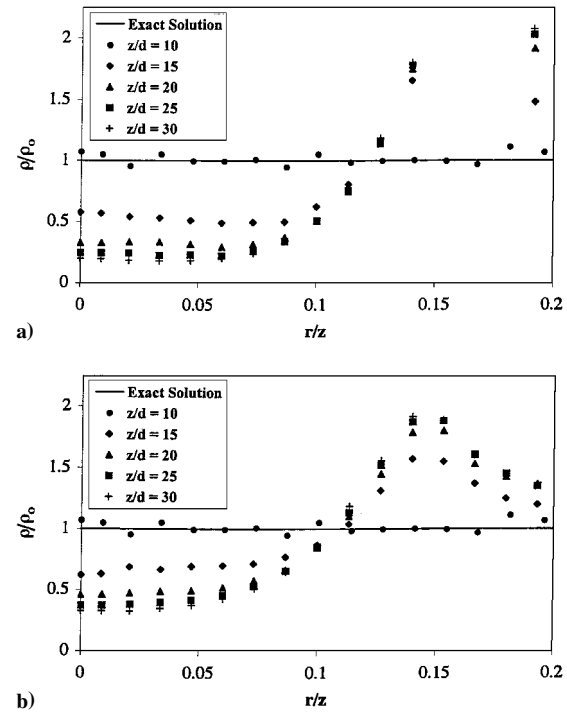

Fig. 12 Tracer particle concentration profiles for the jet flow at four downstream locations without the drift correction velocities for a) DRW and b) CRW model.

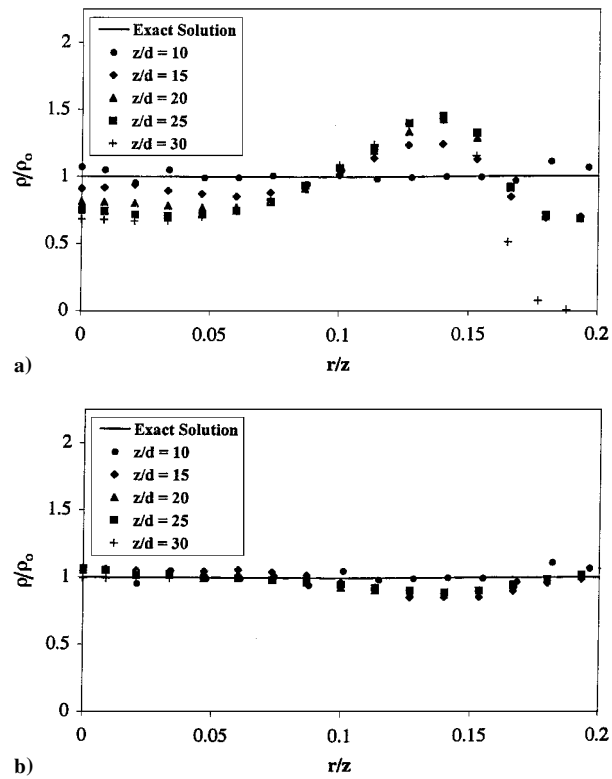

Fig. 13 Tracer particle concentration profiles for the jet flow at four downstream locations for a) DRW model with drift correction proposed by MacInnes and Bracco[6] and b) CRW model with the proposed drift velocity of Eq. (29).

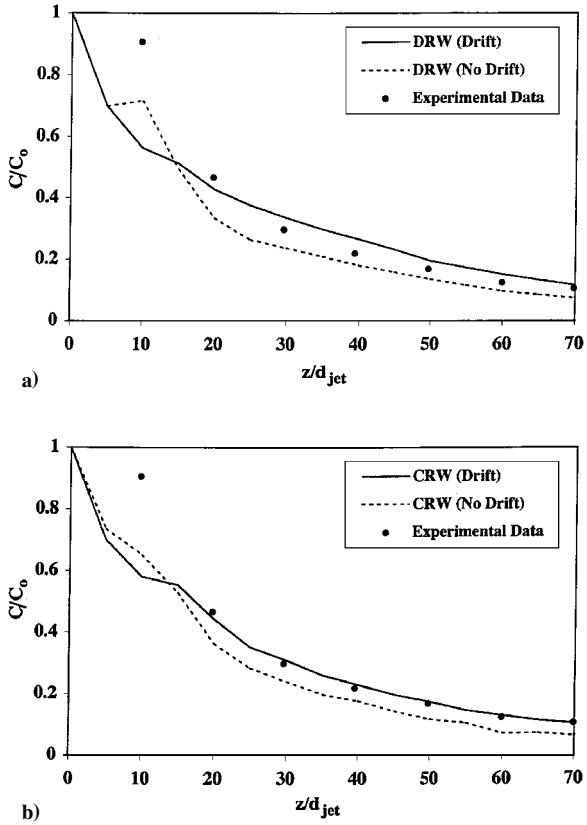

Fig. 14 Comparison of numerical results for the centerline particle concentration of an axisymmetric jet to the experimental data of Yuu et al.[22] for a) DRW model, where the drift of MacInnes and Bracco[6] is utilized, and b) CRW model.

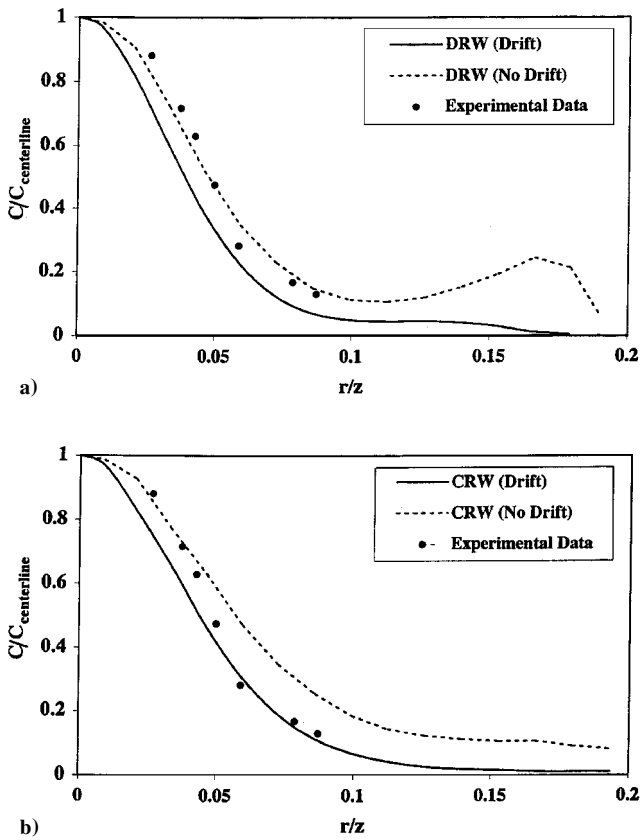

Fig. 15 Comparison of numerical results for the radial particle concentration of an axisymmetric jet to the experimental data of Yuu et al.[22] for a) DRW model, where the drift of MacInnes and Bracco[6] is utilized, and b) CRW model.

suggesting that the drift correction velocity is of order 1% based on Eq. (35).

The axisymmetric jet results shown in Figs. 14 and 15 are for an axisymmetric jet with a jet discharge velocity of 100 m/s and an initial particle Stokes number of 30. Figure 14 shows comparisons for the DRW and CRW models to the experimental data for the centerline particle concentration normalized by the value of the particle concentration at the jet exit. The DRW and CRW simulations without the drift correction underpredict the centerline particle concentration, which is consistent with the particles artificially vacating the centerline region of the jet, where the highest turbulence intensity is located. The CRW model with the drift correction term of Eq. (29) tends to show the best agreement with the data, although the drift-corrected DRW results using Eq. (27) are reasonable.

Figure 15 shows comparisons for the DRW and CRW models to the experimental data for the radial particle concentration at an axial location of $z/d_{\text{jet}} = 50$. The overall match of the CRW model with drift correction to the data of Yuu et al.[22] is again reasonable. Neglecting the drift correction term results in particles incorrectly accumulating in the outer region of the jet where the smallest turbulence intensity is located. This is especially dramatic in the DRW model shown in Fig. 15a, where a large nonphysical spike in the concentration profile at $r/z \sim 0.175$ (similar to the earlier results found for massless particles in a jet shown in Fig. 3). A second test condition at 50 m/s is described by Bocksell and Loth[5] and exhibited similar results. Thus, DRW models by Gosman and Ioannides,[8] Yuu et al.,[22] Schuen et al.,[7] and DeAngelis et al.,[26] which do not include this drift velocity, may have difficulty simulating particle diffusion for flows with strongly inhomogeneous turbulence.

IV. Conclusions

DRW and CRW models were investigated to simulate heavy particle diffusion in free-shear flows. These DRW and CRW models were designed to incorporate the three primary features of turbulent particle diffusion: the crossing-trajectory effect, the continuity effect, and the inertial-limit effect. For the sake of comparison and consistency, both the DRW and CRW models did not include off-diagonal correlation terms and used the same anisotropic turbulence intensities. The calibrated performance for the grid-generated turbulent flow was reasonable for both models, and local time stepping significantly reduced CPU time for the CRW model. The drift correction velocities for the DRW and CRW models were validated in an idealized one-dimensional inhomogeneous channel flow and an empirical two-dimensional inhomogeneous jet flow. The results showed that the present analytical drift correction velocity for the CRW model performed the best, whereas the present analytical DRW correction also gave reasonable results for just the idealized channel flow. The resulting DRW and CRW models also provided reasonable particle diffusion predictions for the Yuu et al.[22] turbulent axisymmetric jet experiment. However, the CRW model again performed better, particularly with respect to correcting for the nonphysical drift due to inhomogeneous turbulence.

Acknowledgments

This work was supported by the Office of Naval Research under Grant N00014-96-1-03412 with Edwin Rood as Technical Monitor and by NASA Lewis Research Center under Contract NAS3-97011 with Thomas Irvine as Technical Monitor. The National Center for Supercomputing Applications computer facilities were utilized in this research.

References

[1] Stock, D. E., "Particle Dispersion in Flowing Gases—1994 Freeman Scholar Lecture," *Journal of Fluids Engineering*, Vol. 118, March 1996, pp. 4–17.

[2] Loth, E., "Numerical Approaches to Dilute Two-Phase Flow," *Progress in Energy and Combustion Science*, Vol. 26, No. 3, 2000, pp. 161–223.

[3] Bocksell, T. L., and Loth, E., "A Random Walk Model for Bubbles and Particles," American Society of Mechanical Engineers, ASME Paper FEDSM99-7366, July 1999.

[4] Csanady, G. T., "Turbulent Diffusion for Heavy Particles in the Atmosphere," *Journal of Atmospheric Sciences*, Vol. 20, May 1963, pp. 201–208.

[5]Bocksell, T. L., and Loth, E., "An Enhanced Discontinuous Random Walk Model for Particle Diffusion in Wakes and Jets," *International Conference on Multiphase Flow*, June 1998.

[6]MacInnes, J. M., and Bracco, F. V., "Stochastic Particle Dispersion Modeling and the Tracer-Particle Limit," *Physics of Fluids A*, Vol. 12, Dec. 1992, pp. 2809–2824.

[7]Schuen, J.-S., Chen, L.-D., and Faeth, G. M., "Evaluation of a Stochastic Model of Particle Dispersion in a Turbulent Round Jet," *AIChE Journal*, Vol. 29, No. 1, 1983, pp. 396–404.

[8]Gosman, A. D., and Ioannides, E., "Aspects of Computer Simulation of Liquid-Fueled Combustors," AIAA Paper 81-0323, 1981.

[9]Townsend, A. A., *The Structure of Turbulent Shear Flow*, Cambridge Univ. Press, Cambridge, England, U.K., 1956.

[10]Batchelor, G. K., *The Theory of Homogeneous Turbulence*, Cambridge Univ. Press, Cambridge, England, U.K., 1953, pp. 34–54.

[11]Wang, L. P., and Stock, D. E., "Numerical Simulation of Heavy Particle Dispersion: Time Step and Nonlinear Drag Considerations," *Journal of Fluids Engineering*, Vol. 114, March 1992, pp. 100–106.

[12]Wells, M. R., and Stock, D. E., "The Effects of Crossing Trajectories on the Dispersion of Particles in a Turbulent Flow," *Journal of Fluid Mechanics*, Vol. 136, 1983, pp. 31–62.

[13]Loth, E., and Stedl, J. L., "Taylor and Lagrangian Correlations in a Turbulent Free Shear Layer," *Experiments in Fluids*, Vol. 26, 1999, pp. 1–6.

[14]Elghobashi, S., and Truesdell, G. C., "Direct Simulation of Particle Dispersion in a Decaying Isotropic Turbulence," *Journal of Fluid Mechanics*, Vol. 242, Sept. 1992, pp. 655–700.

[15]Snyder, W. H., and Lumley, J. L., "Some Measurements of Particle Velocity Autocorrelation Functions in a Turbulent Flow," *Journal of Fluid Mechanics*, Vol. 48, July 1971, pp. 41–71.

[16]Shirolkar, J. S., Coimbra, C. F. M., and Quirez McQuay, M., "Fundamental Aspects of Modeling Turbulent Particle Dispersion in Dilute Flows," *Progress in Energy and Combustion Science*, Vol. 22, 1996, pp. 363–399.

[17]Berlemont, A., Desjonqueres, P., and Gouesbet, G., "Particle Lagrangian Simulation in Turbulent Flows," *International Journal of Multiphase Flow*, Vol. 16, 1990.

[18]Crowe, C. T., Sommerfeld, M., and Tsuji, Y., *Multiphase Flows with Droplets and Particles*, CRC Press, Boca Raton, FL, 1998, pp. 191–203.

[19]Legg, B. J., and Raupach, M. R., "Markov-Chain Simulation of Particle Dispersion in Inhomogeneous Flows: The Mean Drift Velocity Induced by a Gradient in the Eulerian Velocity Variance," *Boundary-Layer Meterology*, Vol. 24, March 1982, pp. 3–13.

[20]White, F. M., *Viscous Fluid Flow*, McGraw–Hill, New York, 1991, pp. 470–480.

[21]Wygnanski, I., and Fiedler, H., "Some Measurements in the Self-Preserving Jet," *Journal of Fluid Mechanics*, Vol. 38, 1969, pp. 577–612.

[22]Yuu, S., Yasukouchi, N., Hirosawa, Y., and Jotaki, T., "Particle Turbulent Diffusion in a Dust Laden Round Jet," *AIChE Journal*, Vol. 24, No. 3, 1978, pp. 509–519.

[23]Bocksell, T. L., "An Enhanced DRW Model for Turbulent Particle Diffusion," M.S. Thesis, Univ. of Illinois, Urbana, IL, 1998.

[24]Anderson, D. A., Tannehill, J. C., and Pletcher, R. H., *Computational Fluid Mechanics and Heat Transfer*, Hemisphere, New York, 1984, pp. 221–235.

[25]Maxey, M. R., and Riley, J. J., "Equation of Motion for a Small Rigid Sphere in a Nonuniform Flow," *Physics of Fluids*, Vol. 26, No. 4, 1983, pp. 883–889.

[26]DeAngelis, B. C., Loth, E., Lankford, D., and Bartlett, C. S., "Computations of Turbulent Droplet Dispersion for Wind Tunnel Tests," *Journal of Aircraft*, Vol. 34, No. 2, 1997, pp. 213–219.

[27]Graham, D. I., "Improved Eddy Interaction Models with Random Length and Time Scales," *International Journal of Multiphase Flow*, Vol. 24, No. 2, 1998, pp. 12–17.

[28]Chen, X. Q., and Pereira, J. C. F., "Comparisons of the Various Particle Dispersion Models in Plane Mixing Shear Layers," *Numerical Methods in Multiphase Flows*, FED Vol. 185, American Society of Mechanical Engineers, Fairfield, NJ, 1994, pp. 217–225.

[29]Iliopoulos, I., and Hanratty, T. J., "Turbulent Dispersion in a Non-Homogeneous Field," *Journal of Fluid Mechanics*, Vol. 32, 1999, pp. 45–71.

[30]Tu, J. Y., and Fletcher, C. A. J., "An Improved Model for Particulate Turbulence Modulation in Confined Two-Phase Flows," *International Communications in Heat and Mass Transfer*, Vol. 21, 1994, pp. 775–783.

M. Samimy
Associate Editor